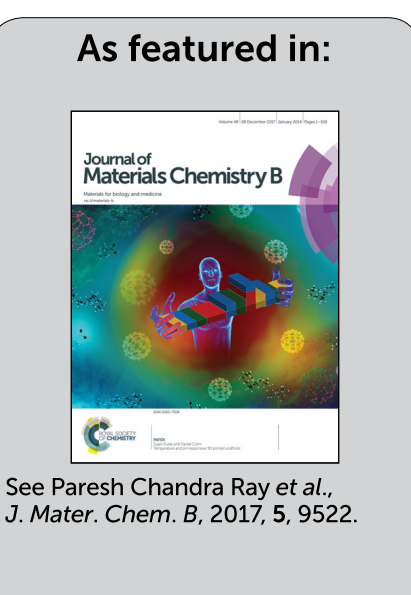


Showcasing bio-inspired 3D architecture research from Dr Ray's Lab in the Department of Chemistry, Jackson State University, Jackson, MS, USA.

A bio-conjugated chitosan wrapped CNT based 3D nanoporous architecture for separation and inactivation of *Rotavirus* and *Shigella* waterborne pathogens

The manuscript describes the development of a bio-inspired 3D architecture using CNT-chitosan composites for the separation of virus and bacteria from water.





Journal of Materials Chemistry B



PAPER

View Article Online
View Journal | View Issue



Cite this: *J. Mater. Chem. B,* 2017, **5**, 9522

A bio-conjugated chitosan wrapped CNT based 3D nanoporous architecture for separation and inactivation of *Rotavirus* and *Shigella* waterborne pathogens

Avijit Pramanik,^a Stacy Jones,^a Ye Gao, Da Carrie Sweet,^a Salma Begum,^a Manoj K. Shukla,^b Janice Paige Buchanan,^b Robert D. Moser^b and Paresh Chandra Ray Da **

The United Nations (UN) estimates that more than one billion people in this world do not have access to safe drinking water due to microbial hazards and it kills more than 7.6 million children every year via waterborne diseases. Driven by the need for the removal and inactivation of waterborne pathogens in drinking water, we report the chemical design and details of microscopic characterization of a bioconjugated chitosan attached carbon nanotube based three dimensional (3D) nanoporous architecture, which has the capability for effective separation and complete disinfection of waterborne pathogens from environmental water samples. In the reported design, chitosan, a biodegradable antimicrobial polysaccharide with an architecture-forming ability has been used for the formation of 3D pores as channels for water passage, as well as to increase the permeability on the inner and outer architectures for killing Rotavirus and Shigella waterborne pathogens. On the other hand, due to their large surface area, CNTs have been wrapped by chitosan to enhance the adsorption capability of the architecture for the separation and removal of pathogens from water. The reported data show that the anti-Rotavirus VP7 antibody and LL-37 antimicrobial peptide conjugated chitosan-CNT architecture can be used for efficient separation, identification and 100% eradication of Rotavirus and Shigella waterborne pathogens from water samples of different sources. A detailed mechanism for the separation and inactivation of waterborne pathogens using the bio-conjugated chitosan based 3D architecture has been discussed using microscopic and spectroscopic studies. Reported experimental data demonstrate that the multifunctional bio-conjugated 3D architecture has good potential for use in waterborne pathogen separation and inactivation technology.

Received 26th October 2017, Accepted 16th November 2017

DOI: 10.1039/c7tb02815f

rsc.li/materials-b

1. Introduction

Although water is essential to human life, as per the World Health Organization (WHO), around 25% of the global population does not have access to drinking water, which is free from microbial hazards.^{1,2}

The United Nations Children's Fund (UNICEF) estimated that unsafe water is responsible for 7.6 million deaths of children under the age of five.^{3,4} As per the Centers for Disease Control (CDC), waterborne pathogens cause significant disease burden to our society, which results in a global economic loss of US\$260 billion annually.^{5–8} It is now well documented that water contaminated with *Rotavirus*, a double-stranded RNA

virus, is the leading cause of death among young children. Similarly, *Shigella* is known to be one of the most contagious types of bacteria which is commonly responsible for waterborne outbreaks in the USA and deaths among infants in our society. Since the average size of the *Rotavirus* is about 80 nm, whereas the pore size of a point-of-use filter varies from 100 nm to 5 microns, *Rotavirus* from infected water cannot be removed using a point-of-use filter. To tackle the above challenges, here we report the chemical design of a chitosan attached carbon nanotube based three dimensional (3D) nanoporous architecture with an average pore size of 30 nm, which has the capability for effective separation and disinfection of waterborne pathogens from environmental water samples.

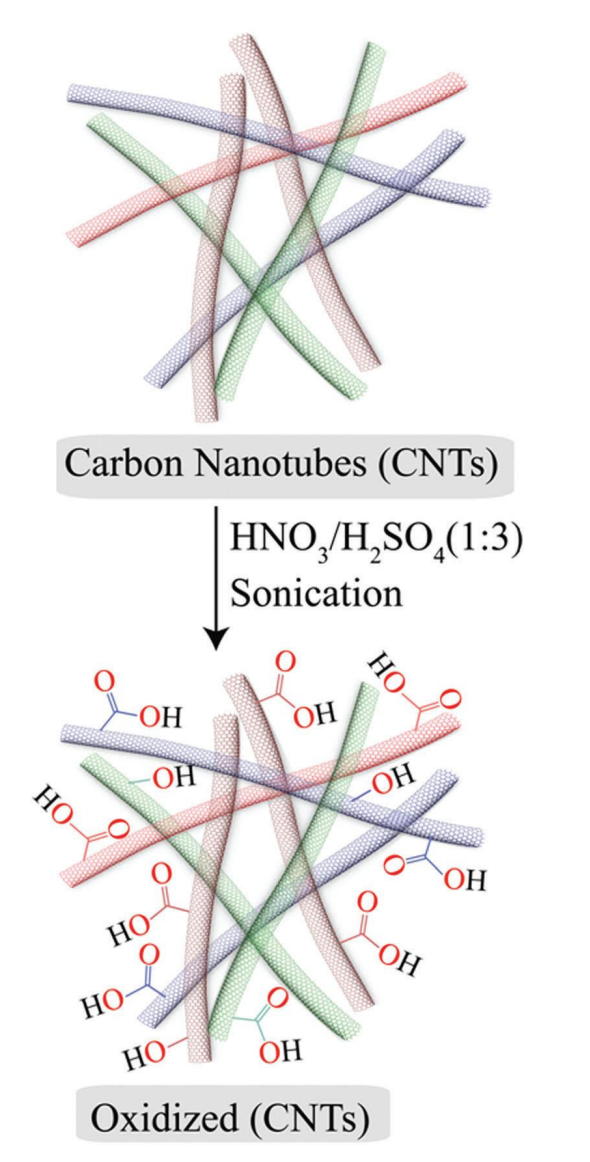
Chitosan, which is composed of β -(1-4)-linked D-glucosamine and *N*-acetyl-D-glucosamine, is a derivative of chitin and it can easily be extracted from the shells of crabs and shrimps. ^{13–20} Due to its good biocompatibility, antibacterial, and gel-forming properties, chitosan biopolymer has been used heavily as

^a Department of Chemistry and Biochemistry, Jackson State University, Jackson, MS, USA. E-mail: paresh.c.ray@jsums.edu; Fax: +1 6019793674

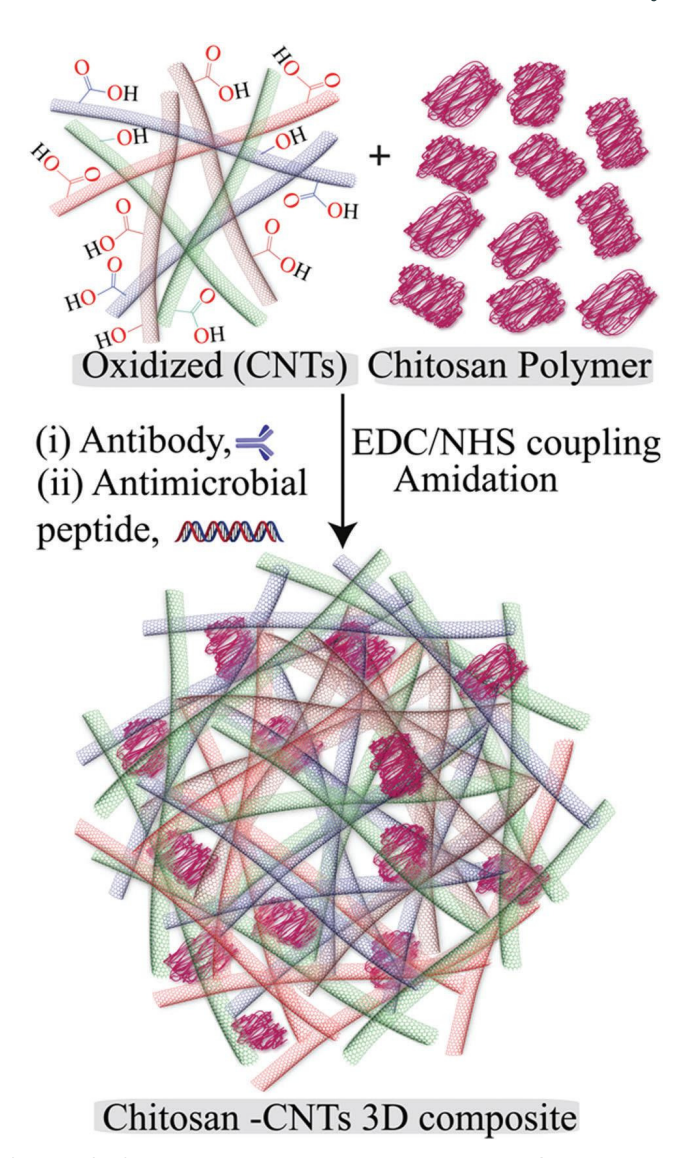
^b US Army Engineer Research and Development Center, 3909 Halls Ferry Road, Vicksburg, MS, USA

biomaterials in the fields of biomedical engineering and biotechnology. 13-28 As shown in Schemes 1 and 2, in our design, chitosan has been used for the formation of a 3D nanoporous architecture as channels for water passage. Due to its strong chelating ability and cationic characteristics, the same chitosan has also been used to increase the permeability on the inner and outer architectures for killing Rotavirus and Shigella. Due to their high specific surface area and very good mechanical strength, single-walled carbon nanotube (SWNT) based architectures have received huge attention for the last decade.²⁹⁻⁴⁵

The Rotavirus structure is well documented in the literature, which is composed of an RNA genome capsid, consisting of six classes of proteins. 46-48 Since the Rotavirus's outer capsid layer contains VP4 and VP7 proteins, the anti-Rotavirus VP4 antibody or anti-Rotavirus VP7 antibody has been used for neutralization of Rotavirus. 46-48 In our design, for 100% neutralization of captured Rotavirus by the 3D nanoporous architecture, we have



Scheme 1 Synthetic procedure we used to develop water dispersible oxidized CNTs.



Scheme 2 Synthetic procedure used to develop a chitosan-CNT architecture.

used the anti-Rotavirus VP7 antibody attached chitosan-CNT architecture. The antimicrobial peptide LL-37 is a multifunctional host defense peptide which is known to kill Shigella. 49-52

It has been well documented that LL-37 interacts with lipid bilayers via electrostatic interaction with Shigella bacterial surfaces and forms pores, leading to the osmotic lysis of the bacterial cell. $^{49-52}$ In our design, for 100% killing of captured *Shigella* by the 3D nanoporous architecture, we have used the LL-37 antimicrobial peptide attached chitosan-CNT architecture. Our reported data demonstrate that the bio-conjugated chitosan-CNT architecture can be used for efficient separation, identification and eradication of Rotavirus and Shigella waterborne pathogens in water samples of different sources.

2. Experimental

Single-walled carbon nanotubes, chitosan, 1-ethyl-3-[3-(dimethylamino)propyl]carbodiimide hydrochloride, poly(ethylene glycol), HNO₃, H₂SO₄, KMnO₄, and other chemicals were purchased from Fisher Scientific and Sigma-Aldrich. *Rotavirus* (ATCC[®] VR-2550[™]), *Shigella* (ATCC[®] 700930[™]) and growth media were purchased from the American Type Culture Collection.

2.1. Development of water-soluble SWCNTs

For the chemical design of a chitosan–CNT architecture, first, we synthesized water soluble carbon nanotubes (CNTs). In order to do this, SWCNTs (5 mg mL $^{-1}$) were dispersed by ultrasonication, and then we performed oxidative treatments using a 3:1 ratio of concentrated sulfuric acid and nitric acid, as shown in Scheme 1. As we and others reported before, $^{29-45}$ during the oxidation treatments, SWCNTs were chemically functionalized with the carboxyl group, which produced $-\mathrm{CO}_2\mathrm{H}$ functionalized SWCNTs, as shown in Scheme 1. TEM data indicate that the average diameter of the water-soluble SWCNTs is about 6–8 nm and length is about 1–6 $\mu\mathrm{m}$. The Raman data indicate a strong D-band at $\sim 1345~\mathrm{cm}^{-1}$ and a G-band at $\sim 1625~\mathrm{cm}^{-1}$. Water solubility is around 0.5 mg mL $^{-1}$.

2.2. Development of a chitosan-CNT 3D architecture membrane

For the design of a chitosan-CNT 3D architecture membrane, we used a cross linking method to covalently conjugate the amine group of chitosan and the -CO₂H group of the SWCNT using 1-ethyl-3-(3-dimethylaminopropyl)carbodiimide (EDC) as a cross linker. For this purpose, first, 0.1 g low molecular weight chitosan was dissolved by adding 0.25 mL of glacial acetic acid to 20 mL of water. After that, the mixture was sonicated vigorously for an hour. In the next step, we removed any undissolved particles by centrifugation. In the next step, 0.05 g of water soluble -CO₂H functionalized SWCNTs was added to a chitosan solution. As shown in Scheme 2, in the next step we added 2 mL of 0.2 molar (M) EDC and 0.05 M N-hydroxysulfosuccinimide sodium salt [1:3 (v/v) ratio], and then the mixture was sonicated for 30 minutes. After that, the sample was kept in an oil bath at about 80 °C under a hood for 90 min. Once the reaction was over, we performed sonication for an hour and a half. After sonication, we obtained a semisolid product, which was used to develop a 10 imes 10 cm size chitosan-CNT 3D architecture membrane. For this purpose, the semisolid product was used for spin-casting at 1500 rpm onto a glass substrate. Finally, it was vacuum-dried overnight at 60 °C and the 3D architecture membrane was removed from the glass substrate. To understand the chitosan attachment on the CNT architecture, we recorded the infrared (IR) spectra of the freshly prepared chitosan-CNT architecture and compared the data with those of only CNTs as reported in Fig. 1C1 and C2. For this purpose, the samples were placed on the ATR (attenuated total reflection) crystal. After that, the IR spectra of the synthesized compounds were recorded using a Perkin-Elmer-spectrum Two FT-IR spectrometer in the 4000-400 cm⁻¹ range. As reported in Fig. 1C, FTIR data of the chitosan-CNT architecture clearly show the presence of an amide-A band due to the -N-H stretching, mainly, an amide I band due to the C=O bond stretching, an amide II band due to the in-plane NH bending, an OH stretching band, a C-O-C stretching band and a polysaccharide band.

The presence of all the amide bands in the FTIR spectra of the chitosan–CNT architecture clearly shows the attachment of the chitosan–CO₂H functionalized SWCNTs. The Raman spectra of the chitosan–CNT architecture shows a strong D-band at $\sim 1345~{\rm cm}^{-1}$ and a G-band at $\sim 1625~{\rm cm}^{-1},^{30-40}$ which clearly indicate the presence of CNTs on the architecture, and stronger D bands show that the modification extent for CNTs is high.

2.3. Development of an anti-*Rotavirus* VP7 antibody and an LL-37 antimicrobial peptide conjugated chitosan–CNT architecture

For 100% neutralization of captured *Rotavirus* and complete killing of *Shigella* by the 3D nanoporous architecture, we have developed an anti-*Rotavirus* VP7 antibody and an LL-37 antimicrobial peptide attached chitosan–CNT architecture. For this purpose, initially, the anti-*Rotavirus* VP7 antibody and the LL-37 antimicrobial peptide were bio-conjugated with CNTs *via* the –CO₂H group by amide linkage using 1-ethyl-3-[3-(dimethylamino)propyl]carbodiimide hydrochloride as the crosslinking agent in the presence of *N*-hydroxysulfosuccinimide sodium salt, using a previously reported method. ^{11,24} For this purpose, we used 1 mg of the anti-*Rotavirus* VP7 antibody, 80 mg of the LL-37 antimicrobial peptide, 0.1 g of low molecular weight chitosan, 0.25 mL of glacial acetic acid in 20 mL of water and 0.05 g of water soluble –CO₂H functionalized SWCNTs.

All mixtures were kept in an oil bath at about 60 °C under a hood for 80 min. After sonication for one and a half hours, we obtained a semisolid product, which was used to develop the anti-Rotavirus VP7 antibody and LL-37 antimicrobial peptide attached chitosan-CNT architecture. To determine the amounts of the Rotavirus VP7 antibody and LL-37 antimicrobial peptide attached to the prepared bio-conjugated chitosan attached carbon nanotubes, we used the Cy3 dye attached Rotavirus VP7 antibody and the FITC dye attached LL-37 antimicrobial peptide. After sonication, the unreacted Rotavirus VP7 antibody and LL-37 antimicrobial peptide were separated by centrifugation. From the fluorescence analysis, we found that around 80% of the Rotavirus VP7 antibody was attached to the architecture and around 75% of the LL-37 antimicrobial peptide was attached to the architecture. After developing the porous architecture, we used a JEM-2100F TEM, high-resolution SEM using a Hitachi 5500 SEM, energy-dispersive X-ray spectroscopy (EDX) analysis and the Brunauer-Emmett-Teller (BET) experiment to characterize product materials, as shown in Fig. 1.

2.4. Characterization of the bio-conjugated chitosan-CNT architecture

As shown in Fig. 1A, the TEM image of the freshly made anti-Rotavirus VP7 antibody and LL-37 antimicrobial peptide conjugated chitosan–CNT architecture shows the porous structure of our architecture. We also performed EDX mapping; this is shown in Fig. 1B1–B3, which show the presence of C, N and O, which indicate the presence of chitosan, the peptide and the antibody with CNTs in the architecture. To determine the specific surface area for the anti-Rotavirus VP7 antibody and LL-37 antimicrobial peptide conjugated chitosan–CNT architecture, we used

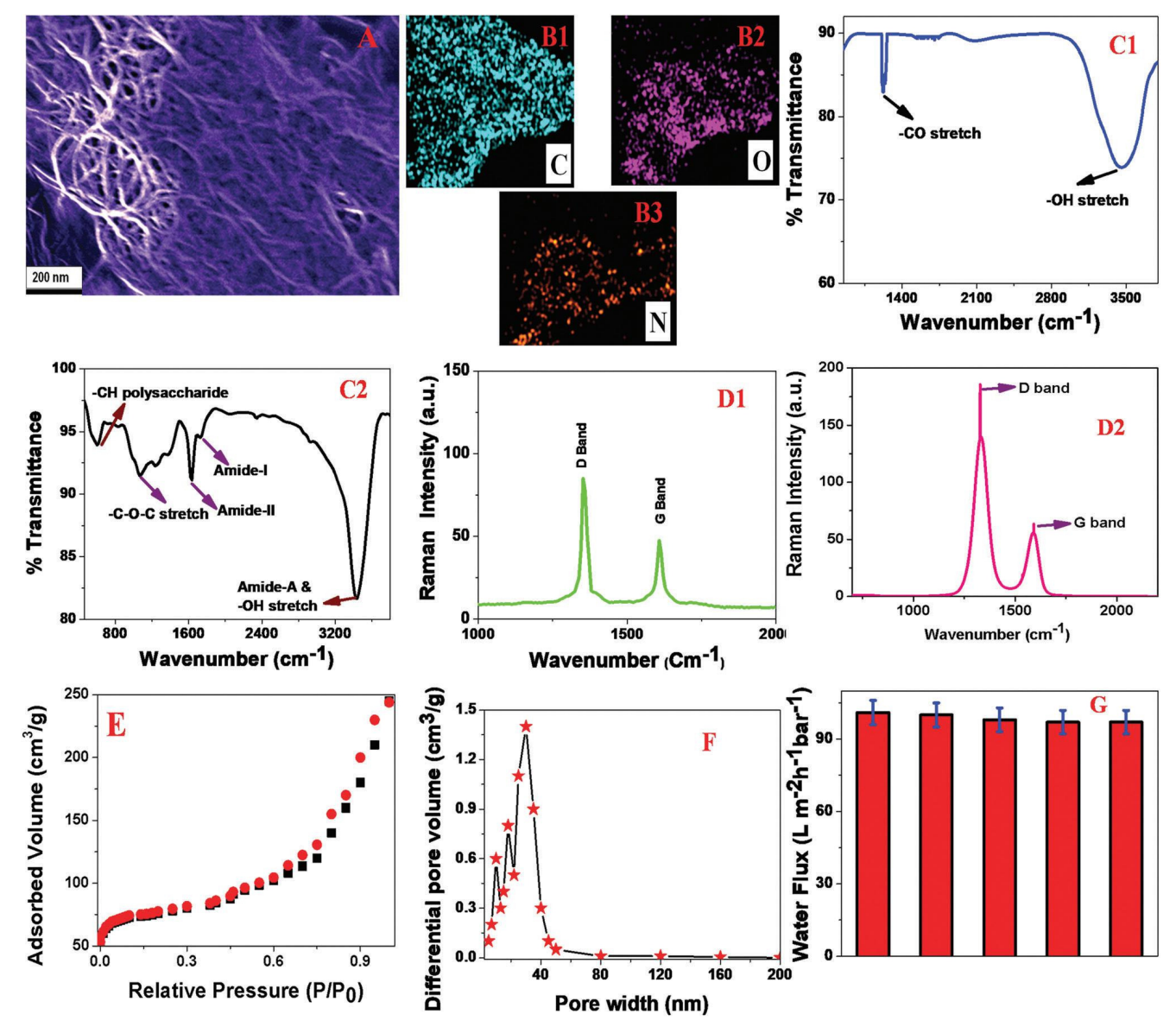


Fig. 1 (A) SEM image of the freshly made anti-Rotavirus VP7 antibody and LL-37 antimicrobial peptide attached chitosan-CNT architecture shows the morphology of the nanoporous architecture. (B) EDX data of the freshly made anti-Rotavirus VP7 antibody and LL-37 antimicrobial peptide attached chitosan-CNT architecture show the presence of C, O, and N. (C1) IR spectrum of the freshly made water soluble SWCNTs shows the presence of -OH stretch and -CO stretch vibrational bands. (C2) IR spectrum of the freshly made chitosan-CNT architecture shows the presence of amide-A, amide-I, amide-II, -OH stretch, -CH polysaccharide and -C-O-C stretch vibrational bands. (D1) SERS spectrum of the freshly made SWCNTs shows the presence of D and G bands. (D2) SERS spectrum of the freshly made chitosan-CNT architecture shows the presence of D and G bands due to the CNTs. (E) N2 adsorption/desorption isotherms of the freshly made anti-Rotavirus VP7 antibody and LL-37 antimicrobial peptide attached chitosan-CNT architecture indicate type III isotherms. (F) Pore size distributions of the freshly made anti-Rotavirus VP7 antibody and LL-37 antimicrobial peptide attached chitosan-CNT architecture show pore sizes ranging from 5 to 200 nm and the highest density at 30 nm. (G) Plot showing water flux data under 1 bar pressure. Measurement was performed 5 times.

N₂ adsorption/desorption data and the Brunauer-Emmett-Teller (BET) method. For the BET surface area measurement, we used a Tristar II 3020 surface area analyzer (Micromeritics, USA), where N₂ was used as the adsorptive gas. On the other hand, we used the Barrett, Joyner, and Halenda (BJH) method to calculate the pore size distribution from the adsorption/desorption isotherms. As shown in Fig. 1E and F, our reported experimental N₂ adsorption/ desorption data show type IV isotherms. BET analysis reported in Fig. 1E indicates that the specific surface area for the anti-Rotavirus VP7 antibody and LL-37 antimicrobial peptide

conjugated chitosan-CNT architecture is 340 m² g⁻¹, with a pore volume of 0.480 cm³ g⁻¹. The corresponding pore size distribution calculated using the BJH method, as shown in Fig. 1F, shows that the pore size ranges from 5 to 80 nm and the average pore diameter for the anti-Rotavirus VP7 antibody and LL-37 antimicrobial peptide conjugated chitosan-CNT architecture is around 30 nm. For the measurement of the water flux for the chitosan-CNT architecture, we collected the permeated water through the nanoporous architecture using an electronic balance. We repeated the experiment a few times. As shown in Fig. 1G and from the experimental data, the water flux for the conjugated chitosan–CNT architecture was estimated to be 98.6 L m⁻² h⁻¹ bar⁻¹. As shown in Fig. 1G, the water flux performance of the chitosan–CNT architecture slight decreases with the number of cycles. It can be due to the membrane's susceptibility to fouling. In our case, fouling occurs due to the accumulation of microorganisms on the chitosan–CNT architecture surface, which may create biofilms on the membrane surface and decrease the water flux due to the increase in resistance to water permeation. To understand whether CNT fragments can leak in water, we performed water filtration several times using the architecture and then filtered water was analyzed for possible CNT fragments in water. We performed TEM, FTIR, ICP and Raman analysis. We did not find any evidence of CNT fragments in water.

2.5. Raman spectral measurements of the chitosan-CNT architecture

To detect the presence of CNTs in the 3D architecture, we performed Raman experiments using a fiber optic probe based Raman probe with 2 mW power using 785 nm light. Experimental details have been reported before. For Raman data collection from the chitosan–CNT architecture, we used a QE65000 spectrometer from Ocean Optics.

2.6. FT-IR measurements of the chitosan-CNT architecture

To understand the amide bond formation and other chemical composition of the chitosan–CNT architecture, we used a Perkin–Elmer-spectrum Two FT-IR spectrometer, as we reported before.²⁴

2.7. Rotavirus sample preparation

To demonstrate *Rotavirus* separation, capture and disinfection, we purchased *Rotavirus* (ATCC[®] VR-2104[™]) from the ATCC. We cultured the virus using the ATCC protocol as instructed. After that, we performed serial dilutions to obtain virus concentrations between 10^5 and 10 PFU per mL, for preparing *Rotavirus* infected water.

2.8. Fluorescence imaging of *Rotavirus* after capture by the chitosan-CNT architecture

For fluorescence imaging, an Olympus IX71 inverted confocal fluorescence microscope was used. A630 nm wavelength light was used as the excitation source. A SPOT Insight digital camera was used for imaging, and Olympus DP capture software was used for data processing, as we reported before.²⁴

2.9. Finding the percentage of *Rotavirus* separated by the chitosan-CNT architecture

We used the real-time reverse transcriptase polymerase chain reaction assay for the counting of *Rotavirus* separated by the chitosan–CNT architecture.

2.10. Antiviral activity measurements using indirect immunofluorescence assay

The anti-Rotavirus activity of chitosan attached carbon nanotubes was monitored using PK-15 (Vero) cells infected by Rotavirus. We used immunofluorescence study to find the

inhibition effect. For this purpose, the cells were incubated with the anti-*Rotavirus* monoclonal antibody for 75 minutes and then the Pacific Blue dye-conjugated antibody was added and kept for 60 minutes. Lastly, we used a microscope to analyze data from immunofluorescence assay.¹¹

2.11. Shigella sample preparation

To demonstrate *Rotavirus* separation, capture and killing, we purchased *Shigella* from the ATCC (ATCC[®] 700930[™]) and then cultured it according to the ATCC protocol. In the next step, we performed serial dilutions to obtain the *Shigella* concentrations between 10^7 and 10 CFU per mL for preparing *Shigella* infected water.

2.12. Finding the percentage of live *Shigella* before and after separation using the chitosan–CNT architecture

For the determination of the percentage of live *Shigella* bacteria before and after separation using the chitosan–CNT architecture, we used a colony-countable plate. Experimental details have been reported before.²⁴ At the end, the colony counter (Bantex, Model 920 A) was used to determine the amount of live bacteria. We also used the RT-PCR experiment for the counting of pathogens.

3. Results & discussion

3.1. Anti-*Rotavirus* VP7 antibody-conjugated chitosan-CNT architecture for separation and inactivation of *Rotavirus*

To determine whether the bio-conjugated chitosan–CNT architecture can be used for the separation of *Rotavirus* from water, we performed filtration of 50 mL of the water sample containing 6.8×10^5 (plaque-forming units) PFU per mL of *Rotavirus*.

After that, we used the reverse transcription polymerase chain reaction (RT-PCR) to determine the amount of Rotavirus captured by the 3D architecture and also the amount of Rotavirus remaining in the water sample. We also performed an SEM study to characterize the captured Rotavirus. As shown in Fig. 2A, the SEM image clearly shows that a huge number of Rotavirus are clustered above the 3D architecture, which is also confirmed using RT-PCR data. As shown in Fig. 2B, RT-PCR data show that our 3D architecture is able to remove more than 99% of Rotavirus from a water sample. This highly efficient Rotavirus removal is mainly due to the fact that the pore size of the anti-Rotavirus VP7 antibody conjugated chitosan-CNT architecture is around 30 nm, whereas the Rotavirus size is about 80 nm. As a result, during the filtration, water can pass through the architecture very easily, but due to its much bigger size, Rotavirus is captured by the architecture. As we discussed before, Rotavirus is a contagious virus that can cause gastroenteritis, and therefore, not only separation, but inactivation is also very important for society. 1-8 To determine the antiviral potential of our bio-conjugated chitosan attached carbon nanotubes against Rotavirus, we incubated PK-15 cells with 3000 PFU per well of Rotavirus in the presence or absence of bio-conjugated chitosan attached carbon nanotubes. After one day of incubation, the Rotavirus infected PK-15 cells were

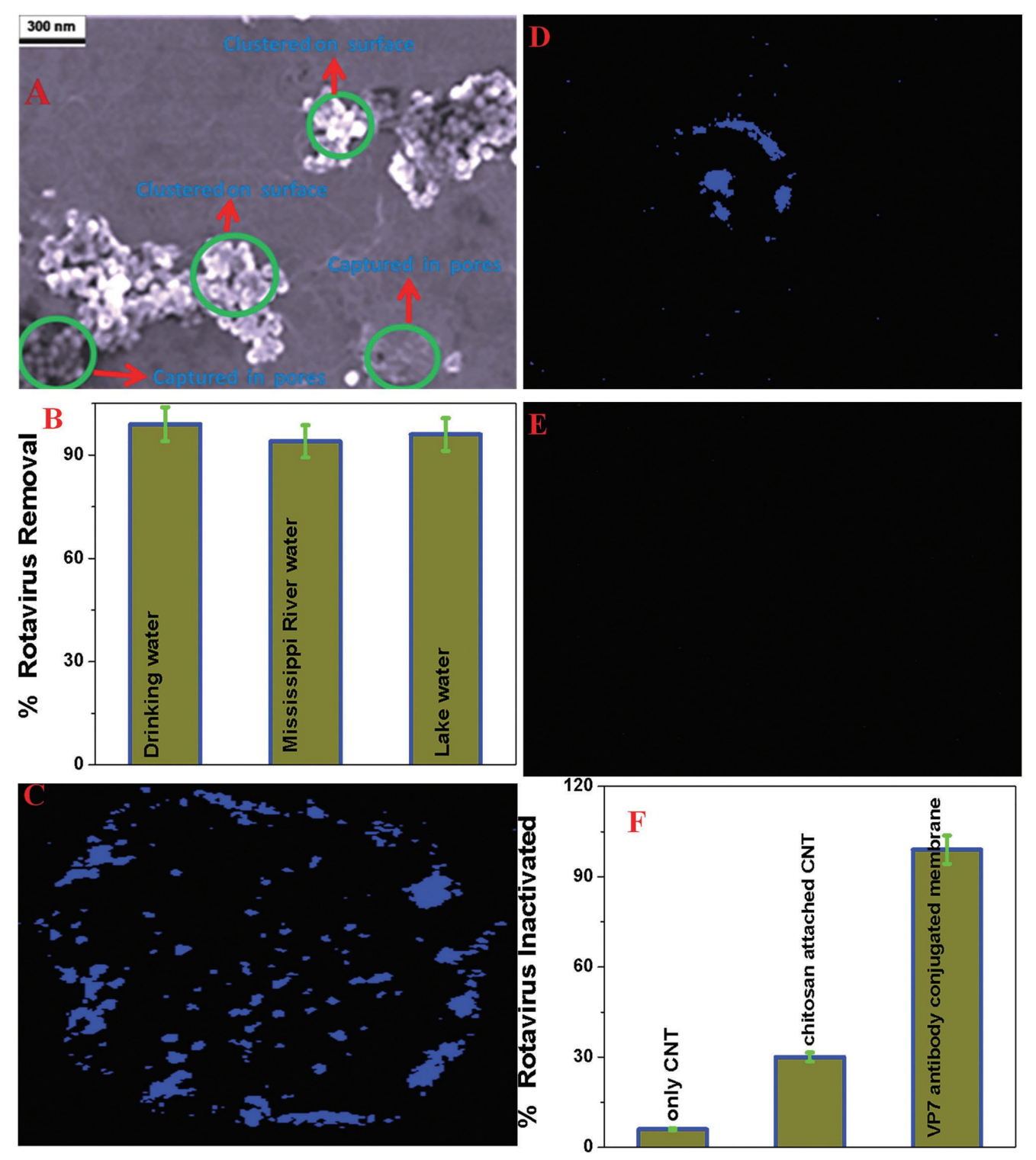


Fig. 2 (A) SEM image shows that Rotavirus has been captured by the anti-Rotavirus VP7 antibody attached chitosan conjugated chitosan-CNT architecture. The SEM image indicates that some of the Rotavirus are clustered on the 3D architecture surface and some of them are captured inside the pores. (B) Plot showing the Rotavirus removal efficiency using the anti-Rotavirus VP7 antibody attached chitosan conjugated chitosan-CNT architecture from drinking water, Mississippi River water and Mississippi lake water. The real-time reverse transcriptase (RT) polymerase chain reaction (PCR) assay was carried out for the counting of Rotavirus. (C) Immunofluorescence assay for Rotavirus-infected Vero cells to find the virus inhibition effect in the absence of the 3D architecture. (D) Immunofluorescence assay for Rotavirus-infected Vero cells, to find the virus inhibition effect in the presence of the chitosan-CNT architecture without the antibody. (E) Immunofluorescence assay for Rotavirus-infected Vero cells, to find the virus inhibition effect in the presence of the anti-Rotavirus VP7 antibody attached chitosan-CNT architecture. (F) Plot showing the Rotavirus inhibition effect in the presence of the CNT architecture, the chitosan-CNT architecture without the antibody and the anti-Rotavirus VP7 antibody attached chitosan-CNT architecture.

immunostained with the blue dye conjugated specific antibody, as we discussed in the Experimental section.

As shown in Fig. 2C and E, the number of *Rotavirus* infected cells significantly decreased in the presence of chitosan attached carbon nanotubes. As reported in Fig. 2E and F, the antiviral activity is around 100%, when the anti-*Rotavirus* VP7 antibody was attached to the chitosan–CNT architecture. The very high antiviral activity observed in the presence of the anti-*Rotavirus* VP7 antibody is due to the fact that VP7 is a glycoprotein which is the major constituent of the outer protein layer of *Rotavirus* ^{46–48} as we discussed before. The anti-*Rotavirus* VP7 antibody shows very strong antiviral activity by decapsidation of the virion and dissociation of the VP7 trimers. ^{46–48} All the above reported data clearly show that the presence of the anti-*Rotavirus* VP7 antibody is very important for the antiviral activity of our 3D architecture.

Next, to determine whether our bio-conjugated chitosan-CNT architecture can be used for the separation of Rotavirus from the environmental water samples, we used Rotavirus infected water from the Mississippi Reservoir and Mississippi River. For this purpose, 100 mL of water was collected from each place of the Mississippi Reservoir and Mississippi River and then the water was infected with 6.8×10^5 PFU per mL of Rotavirus. In the next step, we filtered 50 mL of the Rotavirus infected environmental water sample using a 100 µm thick bioconjugated chitosan-CNT architecture. As we show in Fig. 2B, the efficiency of the removal of Rotavirus from the Mississippi Reservoir and Mississippi River water samples using the bioconjugated chitosan-CNT architecture is about the same as we have observed in the case of drinking water. Fig. 2B also indicates that the efficiency of Rotavirus removal from the drinking water is slightly higher than that from the Mississippi River water, and this is mainly due to the interference from different types of microbes which are present in the Mississippi River water. All microbes are also filtered/captured by the 3D membrane, and as a result, the Rotavirus removal efficiency is slightly less for the Mississippi River water in comparison to the drinking water samples, using the 3D membrane. All the above reported data clearly show that the Rotavirus removal efficiency remains the same with a slight change in pH, humidity, organic impurities, different salts and other metal ions. Next, to understand the efficiency of Rotavirus separation of our developed chitosan-CNT architecture compared to that of the activated carbon filter, we performed filtration of 50 mL of the Rotavirus infected environmental water sample using a activated carbon filter. Since the pore size of the activated carbon filter is more than 100 nm, we observed that less than 20% of the Rotavirus were separated using the activated carbon filter.

3.2. LL-37 antimicrobial peptide conjugated chitosan-CNT architecture for separation and inactivation of *Shigella*

To determine whether the LL-37 antimicrobial peptide conjugated chitosan–CNT architecture can be used for the separation of *Shigella* from water, we performed filtration of 50 mL of the water sample containing 3.1×10^5 (colony-forming units) CFU per mL of *Shigella* using a 100 μ m thick bio-conjugated chitosan–CNT architecture. After that, we used the colony counting

and the reverse transcription polymerase chain reaction (RT-PCR)^{53,54} to determine the amount of Shigella captured by the 3D architecture. As shown in Fig. 3A, the TEM image clearly shows that a huge amount of *Shigella* is captured by the LL-37 antimicrobial peptide conjugated chitosan-CNT architecture. As shown in Fig. 3B, our LL-37 antimicrobial peptide conjugated chitosan-CNT architecture is able to remove 100% of Shigella from the water sample. This highly efficient Shigella removal is mainly due to the fact that the pore size of the LL-37 antimicrobial peptide conjugated chitosan-CNT architecture is around 30 nm, whereas the Shigella size is about 1-2 μm. As a result, during the filtration, water can pass through the architecture very easily, but due to its much bigger size, Shigella is captured by the LL-37 antimicrobial peptide conjugated chitosan-CNT architecture. As shown in Fig. 3B, the efficiency of removal of Shigella from the Mississippi Reservoir and Mississippi River water samples using the LL-37 antimicrobial peptide-conjugated chitosan-CNT architecture is about the same as we have observed in the case of drinking water.

To understand the antimicrobial activity of our architecture, after capturing Shigella using the bio-conjugated chitosan-CNT architecture, we washed the architecture surface thoroughly with water several times. As shown in Fig. 3C-F, almost all Shigella were killed when they were filtered using the LL-37 antimicrobial peptide conjugated chitosan-CNT architecture. The very high antimicrobial activity observed in the presence of the LL-37 antimicrobial peptide conjugated chitosan-CNT architecture is due to several factors and they are as follows: when Shigella is captured by the architecture, there will be a strong interaction between the positively charged chitosan and the negatively charged Shigella cell wall via coordinating lipopolysaccharide, and as a result, cell lysis occurs due to the leakage of the intracellular constituents. On the other hand, it is now well documented that the two hydrophobic domains in LL-37 can bind and disrupt the anionic bacterial architecture surfaces by forming pores. 49-52 Several reported data show that the C-type lectin RegIIIa from the LL-37 antimicrobial peptide can bind bacterial peptidoglycans and facilitate pore formation in the architecture. 49-52 As shown in Fig. 3G, our HRTEM data clearly show the pore formation on the Shigella surfaces, which were captured by the LL-37 antimicrobial peptide conjugated chitosan-CNT architecture. To understand this better, we also performed the same experiment using only the CNT architecture and the chitosan attached CNT architecture and compared the results with the LL-37 antimicrobial peptide conjugated chitosan-CNT architecture. As shown in Fig. 3H, only 7% of Shigella were killed when we used only the CNT architecture. And it is due to the fact that CNTs are known to exhibit antimicrobial activity via damage of the bacterial cell architecture and destabilization of the cytoplasmic architecture. On the other hand, around 55% of Shigella were killed when we used the chitosan attached CNT architecture. We also performed the experiment using only the LL-37 antimicrobial peptide and we found that the killing efficiency was around 52%. All the above results clearly show that 100% of killing efficiency was achieved using the LL-37 antimicrobial peptide conjugated chitosan-CNT

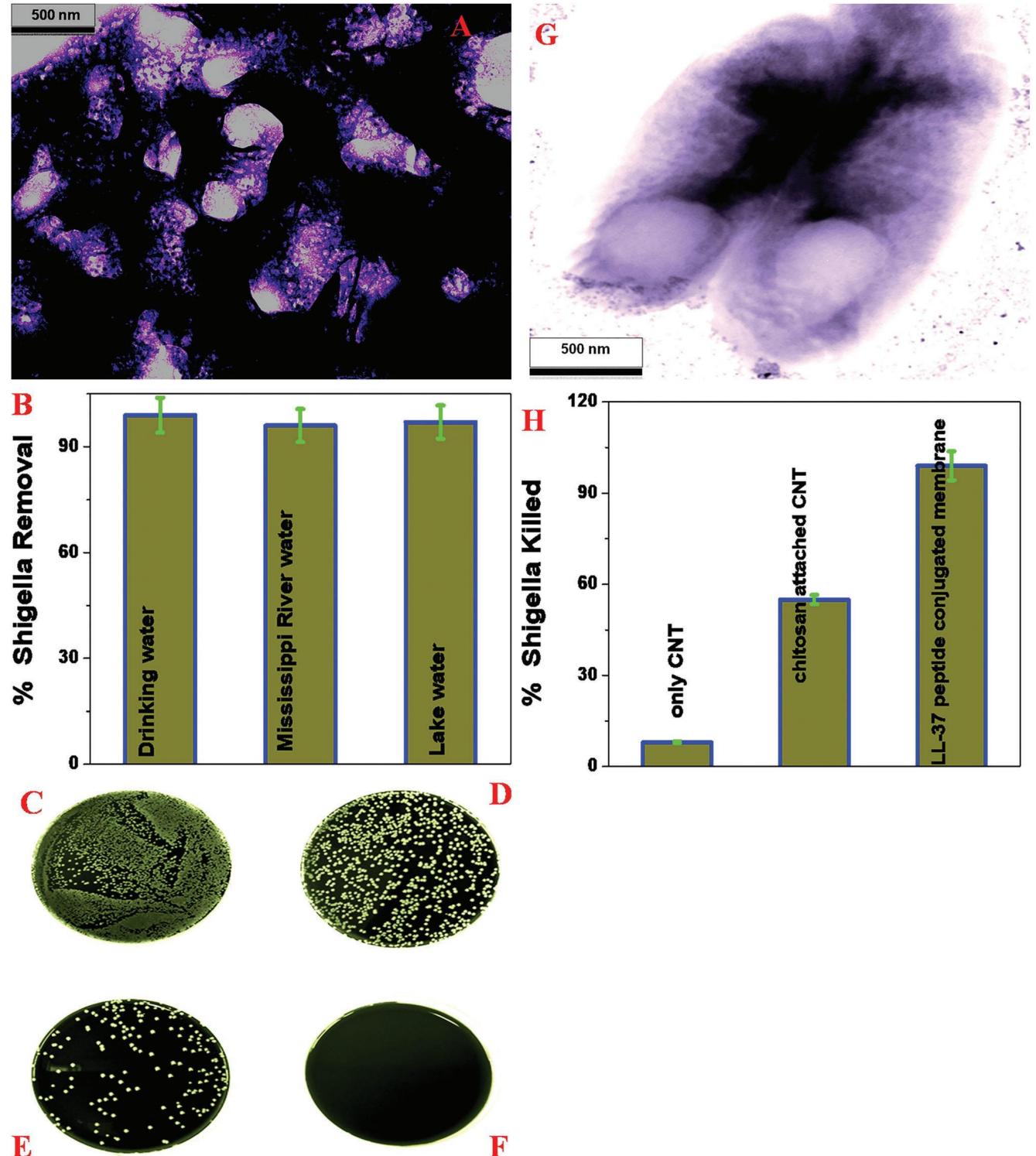


Fig. 3 (A) TEM image of captured Shigella after the removal by the LL-37 antimicrobial peptide conjugated chitosan-CNT architecture. (B) Plot showing the Shigella removal efficiency using the LL-37 antimicrobial peptide conjugated chitosan-CNT architecture from drinking water, Mississippi River water and Mississippi lake water. The real-time reverse transcriptase (RT) polymerase chain reaction (PCR) assay was used for the counting of Shigella. (C-F) Colonies of bacteria showing the amount of live Shigella (C) before filtration using the LL-37 antimicrobial peptide conjugated chitosan-CNT architecture, (D) after filtration using the CNT based architecture, (E) after filtration using the chitosan based architecture and (F) after filtration using the LL-37 antimicrobial peptide conjugated chitosan-CNT architecture. (G) TEM of Shigella after separation by the 3D architecture clearly shows the pore formation on the bacterial surface. In this case, we maintained the acceleration voltage at 70 keV. (H) Plot showing the Shigella inhibition effect in the presence of the CNT architecture, the chitosan conjugated carbon nanotube based three-dimensional nanoporous architecture and the LL-37 and LL-37 antimicrobial peptide conjugated chitosan-CNT architecture. The LL-37 antimicrobial peptide conjugated chitosan-CNT architecture for the separation and inactivation of Shigella.

architecture, where both LL-37 antimicrobial peptide conjugated chitosan and CNT killed *Shigella* using pore forming and other mechanisms as we discussed before.²⁴

4. Conclusions

In conclusion, in this paper we have reported the development of an anti-*Rotavirus* VP7 antibody and an LL-37 antimicrobial peptide conjugated chitosan attached carbon nanotube based porous three-dimensional architecture with a specific surface area of 340 m² g⁻¹, an average pore size of 30 nm and a pore volume of 0.480 cm³ g⁻¹, which can be used for efficient separation and 100% eradication of *Rotavirus* and *Shigella* waterborne pathogens from water samples. Our reported data show that as the pore size of the 3D nanoporous architecture is much lower than those of *Rotavirus* and *Shigella* waterborne pathogens, our bio- conjugated chitosan attached carbon nanotube based porous three dimensional architecture is capable of capturing and separating more than 99% of *Rotavirus* and *Shigella* waterborne pathogens from environmental water samples.

Our reported data indicate that the same anti-Rotavirus VP7 antibody and LL-37 antimicrobial peptide conjugated chitosan attached carbon nanotube based porous three dimensional architecture can be used for 100% total eradication of Rotavirus and Shigella waterborne pathogens. Due to the presence of the anti-Rotavirus VP7 antibody, our 3D architecture exhibits very strong antiviral activity for Rotavirus via decapsidation of the virion and dissociation of the VP7 trimers. Similarly, due to the presence of the strong electrostatic interaction between the positively charged chitosan and the negatively charged Shigella cell wall, and due to the binding of hydrophobic domains in LL-37 and disruption of the anionic Shigella architecture surfaces by pore formation, 100% total eradication of Shigella waterborne pathogens has been observed. Since chitosan is available in nature and a bulk amount of CNTs can be prepared very easily industrially, after proper engineering design, one can easily develop large scale 3D nano-porous architectures using low-cost synthesis methods. Although our reported data show that the CNT-chitosan architecture has enormous potential for the efficient separation and eradication of Rotavirus and Shigella waterborne pathogens, robust synthetic techniques and engineering design are necessary before it can be used for society.

Conflicts of interest

There are no conflicts to declare.

Acknowledgements

Dr Ray is thankful for NSF-PREM grant # DMR-1205194, NSF RII Track-2 FEC grant # 1632899, and ARO grant # W911NF-11-D-0001-0380. The use of trade, product, or firm names in this report is for descriptive purposes only and does not imply endorsement by the U.S. Government. The tests described and the resulting data presented herein, unless otherwise noted, are based upon

work partly supported by the U.S. Army Basic Research Program under PE 61102, Project T22, Task 01 "Military Engineering Basic Re-search". Permission was granted by the Director, EL to publish this information. The findings of this report are not to be construed as an official Department of the Army position unless so designated by other authorized documents.

Notes and references

- 1 World Health Organization (WHO) Water Sanitation and Health, 2015, accessed June 17, 2017.
- 2 http://www.who.int/immunization/diseases/Rotavirus/en, accessed June 17, 2017.
- 3 UNICEF, Progress on Sanitation and Drinking Water—2015 Update and MDG Assessment. World Health Organization; Geneva, Switzerland, 2015.
- 4 World Health Organization UN-Water Global Analysis and Assessment of Sanitation and Drinking-Water (GLAAS) 2024-Report, accessed on 1st June 2017, available online.
- 5 https://www.cdc.gov/Rotavirus/index.html, accessed June 17, 2017.
- 6 https://www.cdc.gov/ncezid/dfwed/waterborne/index.html, accessed June 17, 2017.
- 7 https://www.cdc.gov/Shigella/index.html, accessed June 17, 2017
- 8 Centers for Disease Control and Prevention (CDC) Surveillance for waterborne disease outbreaks associated with drinking water and other nonrecreational water—United States, 2009–2010, Vol. 62, Centers for Disease Control and Prevention (CDC), Atlanta, GA, 2013, pp. 714–720.
- 9 G. F. Craun, J. M. Brunkard, J. S. Yoder, V. A. Roberts, J. Carpenter, T. Wade, R. L. Calderon, J. M. Roberts., M. J. Beach and S. L. Roy, *Clin. Microbiol. Rev.*, 2010, 23, 507–528.
- 10 T. Wardlaw, P. Salama, C. Brocklehurst and M. Chopra, Diarrhoea: why children are still dying and what can be done, *Lancet*, 2010, 375, 870–872.
- 11 Z. Fan, B. Yust, B. O. V. Nellore, S. S. Sinha, R. Kanchanapally, R. A. Crouch, A. Pramanik, S. C. Reddy, D. Sardar and P. C. Ray, J. Phys. Chem. Lett., 2014, 5, 3216–3221.
- 12 S. A. Khan, A. K. Singh, D. Senapati, Z. Fan and P. C. Ray, *Chem. Soc. Rev.*, 2012, **41**, 3193–3209.
- 13 E. I. Rabea, E. T. Badawy, C. V. Stevens, G. Smagghe and W. Steurbaut, *Biomacromolecules*, 2003, 4, 1457–1465.
- 14 H. Wang, J. Qian and F. Ding, J. Mater. Chem. B, 2017, 5, 6986-7007.
- 15 T. Liu, Z. Liu and C. Song, Science, 2012, 336, 1160-1164.
- 16 N. Yan and X. Chen, Nature, 2015, 524, 155-157.
- 17 B. Duan, X. Zheng, Z. X. Xia, X. L. Fan, L. Guo, L. F. Liu, Y. F. Wang and Q. F. Ye, *Angew. Chem.*, *Int. Ed.*, 2015, 54, 5152–5156.
- 18 P. K. S. Mural, B. Kumar, G. Madras and S. Bose, *ACS Sustainable Chem. Eng.*, 2016, **4**, 862–870.
- 19 A. Gandini, T. M. Lacerda, A. J. Carvalho and E. Trovatti, *Chem. Rev.*, 2016, **116**, 1637–1669.

- 20 J. J. Duan, X. C. Liang, J. H. Guo, K. K. Zhu and L. Zhang, Adv. Mater., 2016, 28, 8037-8044.
- 21 A. Konwar, S. Kalita, J. Kotoky and D. Chowdhury, ACS Appl. Mater. Interfaces, 2016, 8, 20625-20634.
- 22 Y. Fang, R. Zhang, B. Duan, M. Liu, A. Lu and L. Zhang, ACS Sustainable Chem. Eng., 2017, 5, 2725-2733.
- 23 R. Kanchanapally, B. P. N. Viraka, S. S. Sinha, F. Pedraza, S. J. Jones, A. Pramanik, S. R. Chavva and C. Tchounwou, RSC Adv., 2015, 5, 18881–18887.
- 24 S. Jones, A. Pramanik, R. Kanchanapally, B. P. V. Nellore, A. Begum, C. Sweet and P. C. Ray, ACS Sustainable Chem. Eng., 2017, 5, 7178-7187.
- 25 H. Acar, J. M. Ting, S. Srivastava, J. L. LaBelle and M. V. Tirell, Chem. Soc. Rev., 2017, 46, 6553-6569.
- 26 S. K. L. Levengood and M. Zhnag, J. Mater. Chem. B, 2014, 2, 3161-3184.
- 27 X. Wei, J. Duan and X. Xu, ACS Sustainable Chem. Eng., 2017, 5, 3195-3203.
- 28 B. P. V. Nellore, R. Kanchanapally, F. Pedraza, S. S. Sinha, A. Pramanik, A. Hamme, Z. Arslan, D. Sardar and P. C. Ray, ACS Appl. Mater. Interfaces, 2015, 7, 19210-19218.
- 29 M. F. L. De Volder, S. H. Tawfick, R. H. Baughman and A. J. Hart, Science, 2013, 339, 535-539.
- 30 R. H. Tunuguntla, F. I. Allen, K. Kim, A. Belliveau and A. Noy, Nat. Nanotechnol., 2016, 11, 639-646.
- 31 R. Das, C. D. Vasitius, A. Schulze, B. Cao, A. F. I. Smail, X. Liu, J. Chen and S. Ramakrishna, Chem. Soc. Rev., 2017, 46, 6946-7020.
- 32 R. Zhang, Y. Zhang and Y. Wei, Chem. Soc. Rev., 2017, 46, 3661-3715.
- 33 W. Duan, A. Ronen, S. Walker and D. Jassby, ACS Appl. Mater. Interfaces, 2016, 8, 22574.
- 34 S. S. Gupta, I. Chakraborty, S. M. Maliyekkal, T. Adit Mark, D. K. Pandey, S. K. Das and T. Pradeep, ACS Sustainable Chem. Eng., 2015, 3, 1155-1163.
- 35 J. M. Schnorr and T. M. Swager, Chem. Mater., 2011, 23, 646-657.
- 36 L. Beqa, Z. Fan, A. K. Singh, D. Senapati and P. C. Ray, ACS Appl. Mater. Interfaces, 2011, 3, 3316-3324.

- 37 S. Kumar, M. Williander, J. G. Sharma and B. D. Mailhotra, J. Mater. Chem. B, 2015, 3, 9305-9314.
- 38 R. K. CheedaralaJ., H. Jeon, C. D. Kee and I. K. Oh, Adv. Funct. Mater., 2014, 24, 6005-6015.
- 39 J. Y. Oh, Y. S. Kim, Y. Jung, S. J. Yang and C. R. Park, ACS Nano, 2016, 10, 2184-2192.
- 40 M. K. Shin, B. Lee, S. H. Kim, J. A. Lee, G. M. Spinks, S. Gambhir, G. G. Wallace, M. E. Kozlov, R. H. Baughman and S. J. Kim, Nat. Commun., 2012, 3, 650.
- 41 X. He, W. Gao, L. Xie, B. Li, Q. Zhang, S. Lei, J. M. Robinson, E. H. Hároz, S. K. Doorn, W. Wang, R. Vajtai and P. M. Ajayan, Nat. Nanotechnol., 2016, 11, 633-638.
- 42 P. Chen, T. Y. Xiao, Y. H. Qian, S. S. Li and S. H. A. Yu, Adv. Mater., 2013, 25, 3192-3196.
- 43 Y. Liu, Y. Zhao, B. Sun and C. Chen, Acc. Chem. Res., 2013, 46, 702-713.
- 44 A. Ali, M. Suhail, S. Mathew, M. A. Shah, S. M. Harakeh, S. Ahmad, Z. Kazmi, M. A. R. Alhamdan, A. Chaudhary and G. A. Damanhouri, J. Nanosci. Nanotechnol., 2016, 16, 40–57.
- 45 A. de Juan, Y. Pouillon, L. Ruiz-Gonzalez, A. Torres Pardo, S. Casado, N. Martín, A. Rubio and E. M. Perez, Angew. Chem., Int. Ed., 2014, 53, 5394-5400.
- 46 S. D. Trask, S. M. McDonald and J. T. Patton, Nat. Rev. Microbiol., 2012, 10, 165-177.
- 47 S. D. Trask and K. M. Ogden, Curr. Opin. Virol., 2012, 2, 373-379.
- 48 M. A. Diaz-Salinas, D. Silva-Ayala, S. Lopez and C. F. Arias, J. Virol., 2014, 88, 4389-4402.
- 49 M. N. Melo, R. Ferre and M. A. R. B. Castanho, Nat. Rev. Microbiol., 2009, 7, 245-250.
- 50 Y. Kai-Larsen, P. Luthje, M. Chromek, V. Peters and X. Wang, PLoS Pathog., 2010, 6, e1001010.
- 51 K. A. Henzler Wildman, D. K. Lee and A. Ramamoorthy, Biochemistry, 2003, 42, 6545-6558.
- 52 M. Nishida, Y. Imura, M. Yamamoto, S. Kobayashi, Y. Yano and K. Matsuzaki, Biochemistry, 2007, 46, 14284-14290.
- 53 N. Jothikumar and M. W. Griffiths, Appl. Environ. Microbiol., 2002, 68, 3169-3171.
- 54 A. M. Ibekwe, P. M. Watt, C. M. Grieve, V. K. Sharma and S. R. Lyons, Appl. Environ. Microbiol., 2002, 68, 4853-4862.